

Strong Second-Harmonic Generation in Atomic Layered GaSe

Xu Zhou,^{†,⊥} Jingxin Cheng,^{‡,⊥} Yubing Zhou,^{§,⊥} Ting Cao,^{||} Hao Hong,[†] Zhimin Liao,[†] Shiwei Wu,^{*,‡} Hailin Peng,^{*,§} Kaihui Liu,^{*,†,§} and Dapeng Yu[†]

[†]State Key Laboratory for Mesoscopic Physics, Collaborative Innovation Center of Quantum Matter, School of Physics and [§]Center for Nanochemistry, Beijing Science and Engineering Center for Nanocarbons, Beijing National Laboratory for Molecular Sciences, College of Chemistry and Molecular Engineering, Academy for Advanced Interdisciplinary Studies, Peking University, Beijing 100871, China

[‡]State Key Laboratory of Surface Physics, Key Laboratory of Micro and Nano Photonic Structures (MOE), Collaborative Innovation Center of Advanced Microstructures and Department of Physics, Fudan University, Shanghai 200433, China

^{||}Department of Physics, University of California at Berkeley, Berkeley, California 94720, United States

Supporting Information

ABSTRACT: Nonlinear effects in two-dimensional (2D) atomic layered materials have recently attracted increasing interest. Phenomena such as nonlinear optical edge response, chiral electroluminescence, and valley and spin currents beyond linear orders have opened up a great opportunity to expand the functionalities and potential applications of 2D materials. Here we report the first observation of strong optical second-harmonic generation (SHG) in monolayer GaSe under nonresonant excitation and emission condition. Our experiments show that the nonresonant SHG intensity of GaSe is the strongest among all the 2D atomic crystals measured up to day. At the excitation wavelength of 1600 nm, the SHG signal from monolayer GaSe is around 1–2 orders of magnitude larger than that from monolayer MoS₂ under the same excitation power. Such a strong nonlinear signal facilitates the use of polarization-dependent SHG intensity and SHG mapping to investigate the symmetry properties of this material: the monolayer GaSe shows 3-fold lattice symmetry with an intrinsic correspondence to its geometric triangular shape in our growth condition; whereas the bilayer GaSe exhibits two dominant stacking orders: AA and AB stacking. The correlation between the stacking orders and the interlayer twist angles in GaSe bilayer indicates that different triangular GaSe atomic layers have the same dominant edge configuration. Our results provide a route toward exploring the structural information and the possibility to observe other nonlinear effects in GaSe atomic layers.

Since the discovery of graphene^{1,2} and the rise of MoS₂,^{3,4} two-dimensional (2D) atomic layered materials have come to the central stage of material study due to their distinct properties to the bulk form and potential applications in nanoscience and technology.^{5–10} Recently, nonlinear effects in 2D atomic layered materials have attracted increasing interest. Salient examples include nonlinear optical responses from edge states in MoS₂,¹¹ chiral light emission in WSe₂ induced by nonlinear carrier diffusion shift,¹² and nonlinear valley and spin currents in graphene, transition-metal dichalcogenides, or

GaSe.¹³ The pursuit of strong nonlinear effects in 2D materials is therefore of great importance in expanding their functionalities and potential applications beyond linear effects.

Among the large family of 2D materials, atomic layered GaSe has been receiving intensive attention. Monolayer and few-layer GaSe has high responsibility in photocurrent generation;^{14–18} the thinning of GaSe from bulk to few layers will drive a direct-to-indirect bandgap transition;^{18,19} the hole doping can induce tunable magnetism in monolayer GaSe;²⁰ and appreciable nonlinear spin and valley currents can be generated by electrical bias or temperature gradient in monolayer GaSe.¹³ Especially, as bulk GaSe is a well-known nonlinear crystal with second-order optical nonlinear coefficient 2 orders of magnitude larger than that of the widely used LiNbO₃ crystal,^{21,22} one may expect appreciable nonlinear optical phenomena in thin atomic layered GaSe. Indeed, observations of second-harmonic generation (SHG) in few-layered GaSe sheets were reported early this year, where the emission photon energy exceeded the material bandgap with the signal significantly enhanced by resonating with optical dipole transitions.²³ However, at the monolayer limit and under nonresonant condition, it is still elusive whether SHG signal remains appreciable or not. Herein, for the first time we observed strong SHG signal in monolayer GaSe under the nonresonant condition that both the excitation and emission photon energies were within its optical bandgap. The nonresonant SHG intensity of GaSe is the strongest among all the 2D atomic crystals measured up to day. For instance, at the excitation wavelength of 1600 nm, the SHG signal from monolayer GaSe is 1–2 orders of magnitude larger than that from monolayer MoS₂ under the same excitation power. The strong nonlinear signal enables us to use polarization-dependent SHG intensity and SHG mapping to investigate the structural symmetry information on this material. The monolayer GaSe shows 3-fold lattice symmetry that has a one-to-one correspondence to its geometric triangular shape. The bilayer GaSe exhibits two dominant stacking orders: AA and AB stacking, and their correlation to the interlayer twist angles indicates that the bottom and top layers have the same primary edge configuration.

Received: April 27, 2015

Published: June 10, 2015

In monolayer GaSe, two layers of Ga atoms are sandwiched between two layers of Se atoms in an eclipsed fashion (Figure 1a).^{24,25} The in-plane geometry of monolayer GaSe is a

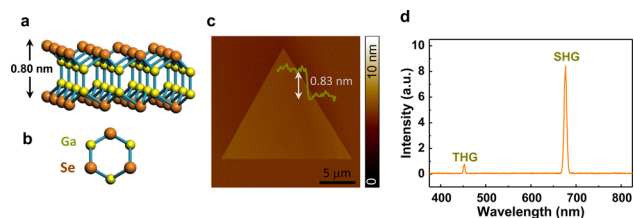


Figure 1. Strong SHG in monolayer GaSe. (a) Schematic atomic structure of monolayer GaSe, two layers of Ga atoms sandwiched by two layers of Se atoms, consisting of vertically stacked Se–Ga–Ga–Se sheets. (b) In-plane configuration of monolayer GaSe is of hexagon structure with Ga atoms and Se atoms separately occupying the two sublattices. (c) AFM image of GaSe monolayer with about 0.83 nm thickness on mica substrate. The monolayer has triangular shape with lateral side length of $\sim 15 \mu\text{m}$. (d) The nonlinear spectrum of monolayer GaSe under excitation of $\lambda_{\text{ex}} = 1350 \text{ nm}$ on fused silica substrate. The peak at 675 and 450 nm corresponds to the SHG and THG signals, respectively.

honeycomb structure in which Ga and Se atoms respectively occupy the two sublattices (Figure 1b). In multilayer GaSe, the adjacent monolayers are coupled by van der Waals interactions. For the monolayer study, in principle one can follow the process of graphite exfoliation method to prepare the sample. However, possibly due to different interlayer coupling strength between GaSe and graphite, no successful mechanical exfoliation of monolayer GaSe has been reported so far.^{22,23} On the other hand, single-crystal GaSe monolayers have been grown on various substrates by chemical vapor deposition (CVD) method^{14–18} (see methods for our growth details in Supporting Information, SI). Figure 1c shows one representative atomic force microscopic (AFM) image of a GaSe monolayer grown on mica. Its height of about 0.83 nm is in consistent with previous reported value for monolayer ($\sim 0.80 \text{ nm}$).¹⁷ The CVD monolayer flake has an equilateral triangular shape, with edge lengths of $\sim 15 \mu\text{m}$ large enough for nonlinear optical measurements.

Monolayer GaSe belongs to noncentrosymmetric D_{3h}^1 space group and therefore should have nonzero SHG signal.^{26–32} But it is unclear whether the signal is strong enough for detection without the excitation power exceeding the materials damage threshold. To investigate the SHG signal from monolayer GaSe, we use a femtosecond OPO laser with tunable wavelength (see setup details in SI). Theoretical calculations within the density functional framework reveal that monolayer GaSe has a bandgap of $\sim 2.3 \text{ eV}$, corresponding to an excitation wavelength of $\sim 540 \text{ nm}$ ^{18,19} (our optical reflection spectrum shows no peak under wavelength longer than 550 nm; see SI for details). In order to investigate the SHG signal under nonresonant conditions for both excitation and emission photon, we purposely tune the laser wavelength longer than twice of monolayer bandgap wavelength. Figure 1d shows one typical nonlinear spectrum of monolayer GaSe under excitation of $\lambda_{\text{ex}} = 1350 \text{ nm}$ on fused silica substrate. The spectrum shows a prominent peak at 675 nm, which is exactly half of the excitation wavelength. Therefore, the observed peak can be unambiguously assigned as SHG signal. (The peak at 450 nm corresponds to a third-harmonic generation, or THG, signal). We measured SHG signal under the other two excitation

wavelengths of $\lambda_{\text{ex}} = 1210$ and 1600 nm . In all these three wavelengths, strong SHG signals were observed (Figure 2a

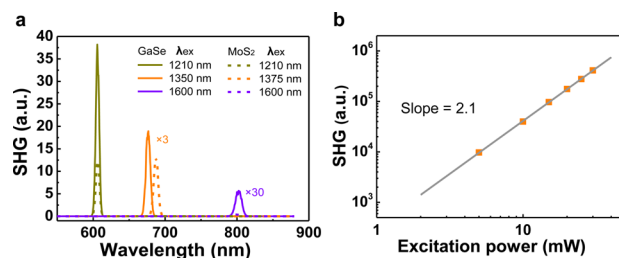


Figure 2. SHG in monolayer GaSe under different wavelengths and excitation power. (a) SHG intensity from monolayer GaSe (solid lines) and MoS_2 (dashed lines) under different excitation wavelengths. The intensity corresponding to $\lambda_{\text{ex}} = 1350$ (1375) and 1600 nm is magnified by 3 and 30 times, respectively. The theoretical optical bandgap of monolayer GaSe is around 540 nm , and the laser with two-photon emission wavelength closer to it generates stronger SHG. (b) The excitation power dependence of SHG intensity. The diagram is a plot of the natural logarithm. The SHG intensity shows a power-law dependence on the excitation power with the coefficient fitted to 2.1, which is very close to the theoretical value of 2 from the electric dipole theory.

solid lines), which proves the presence of strong optical nonlinearities in monolayer GaSe in a wide spectral range. Also, the intensity of the SHG signal follows a simple relation with the wavelength of excitation laser: shorter wavelength produces larger intensity. This behavior should be attributed to the fact that the energy of shorter wavelength SHG photon is closer to the optical bandgap of monolayer GaSe or closer to emission resonant condition.

We further investigated the dependence of SHG intensity on the laser excitation power. The electric dipole theory predicts that under the first-order perturbation $I_{\text{SHG}} = |E(2\omega)|^2 \propto |P(\omega)|^2$, where I_{SHG} , $E(2\omega)$ and $P(\omega)$ are the SHG intensity, SHG electric field vector, and excitation power, respectively.³³ As a result, the SHG intensity should show a quadratic dependence on the excitation power. Indeed, in our experiment, we found the exponent is about 2.1 (Figure 2b), which is very close to the theoretical value of 2. This agreement suggests that under our experimental conditions, the simple electric dipole theory describes the SHG phenomenon in monolayer GaSe quite well. In the context of the electric dipole theory, we can quantitatively estimate the optical second-order susceptibility ($\chi^{(2)} = \chi^{(2)}_{\text{bbb}}$) of monolayer GaSe on fused silica substrate,³³ which gives $\sim 2.4 \times 10^{-9}$, 1.7×10^{-9} , and $0.7 \times 10^{-9} \text{ m/V}$ for $\lambda_{\text{ex}} = 1210$, 1350 , and 1600 nm , respectively (see details in SI). In comparison, the GaSe bulk has a $\chi^{(2)}$ of around $1.4 \times 10^{-10} \text{ m/V}$.²² To evaluate the SHG effect of monolayer GaSe qualitatively in the 2D material family, we compared it with monolayer MoS_2 , which has the same symmetry and was widely investigated before. We measured the SHG signal of monolayer MoS_2 under nonresonant condition ($\lambda_{\text{ex}} = 1600 \text{ nm}$), and the intensity is 1–2 orders of magnitude smaller than monolayer GaSe (Figure 2a, purple dashed line). As a matter of fact, under a nonresonant condition and of the same excitation power, the SHG intensity of monolayer GaSe is larger than that of any other 2D monolayer reported so far, including MoS_2 , WS_2 , WSe_2 , and BN .^{26–29} The larger SHG intensity in GaSe monolayer mainly comes from its smaller $n_{2\omega}$ and n_{ω} and also larger $\chi^{(2)}$ and d (see details in SI).

The strong SHG from monolayer GaSe enables us to facilitate this signal to investigate the structural symmetry properties of this material. We first probed the crystalline lattice symmetry in monolayer by polarization-dependent SHG intensity. We detected the SHG intensity with emission field polarization parallel to excitation field. Monolayer GaSe has D_{3h}^1 3-fold symmetry, and therefore for the parallel polarization component, its SHG intensity will exhibit a 6-fold rotational symmetry with SHG intensity varying with azimuthal angle θ (as indicated in Figure 3a).^{26–30} As shown in Figure 3b, the

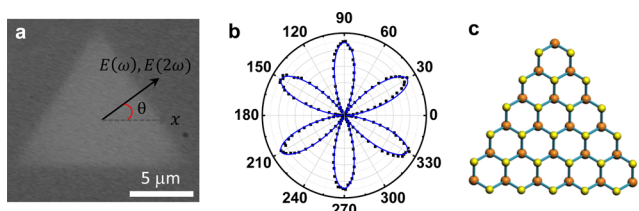


Figure 3. The crystalline symmetry in monolayer GaSe as probed by polarization-dependent SHG intensity. (a) Optical image of a triangular GaSe monolayer on Si/SiO₂ substrate. Azimuthal angle θ is defined as the polarization direction (for both excitation and emission) relative to one triangular lateral side direction. (b) The polarization angle θ dependent SHG intensity. It exhibits a clear six-fold rotational symmetry ($I = I_0 \sin^2(3\theta)$). (c) The crystalline lattice model of monolayer GaSe, derived from the polarization-dependent pattern in (b). It has a one-to-one correspondence to the geometric triangular shape in (a).

polarization-resolved SHG intensity shows a clear six-petal pattern, which directly reveals the underlying symmetry and orientation of GaSe monolayer. This angle dependence can be described as $I = I_0 \sin^2(3\theta)$, where I and I_0 are the SHG intensity and the maximum intensity of SHG response, respectively. From the symmetry analysis of D_{3h}^1 monolayers,^{26–30} the maximum petal direction is parallel to the in-plane Ga–Se or Se–Ga direction. However, though the electrical dipole directions of Ga–Se and Se–Ga bonds are opposite in plane, since the SHG intensity is not phase sensitive, we cannot distinguish between the Ga–Se and Se–Ga bond alignments from the polarization-dependent signal, i.e., we do not know whether the Ga–Se bond direction is parallel or antiparallel to the petal direction yet. Therefore, the equilateral triangular clusters may correspond to clusters with a Se or Ga terminated zigzag edge. We show one possible structural model in Figure 3c.

We further employed the SHG mappings to investigate the stacking orders in GaSe bilayers. In general, the GaSe bilayers can exhibit two stable stacking configurations derived from the bulk crystal structures (ϵ - and β -phase).²² We name the two configurations as AA and AB stacking, following the conventions in bilayer MoS₂.³¹ In the AA stacking case, the in-plane Ga–Se bond direction is the same for the two layers, while in the AB-stacking case, the in-plane Ga–Se bond direction is opposite. AA-stacked bilayer still belongs to noncentrosymmetric D_{3h}^1 group as in monolayer and, therefore, should have a strong SHG signal. The electric dipole theory predicts that the SHG signal in AA-stacked bilayer will be four times that of the monolayer (the SHG electric fields of the two layers are in phase). In contrast, AB-stacked bilayer belongs to the centrosymmetric D_{3d}^1 group and, therefore, has no appreciable SHG signal (the SHG electric fields of the two layers are out of phase). In our CVD samples, the bilayers

predominantly have two configurations with twist angle of $\phi = 0^\circ$ (Figure 4a) and $\phi = 60^\circ$ (Figure 4d), where ϕ is defined as

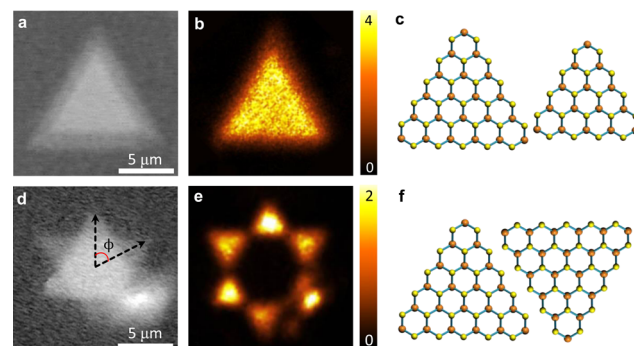


Figure 4. The stacking order in GaSe bilayers as probed by SHG imaging. (a–c) Optical image, SHG mapping, and atomic lattice model for GaSe bilayer with twist angle of $\phi = 0^\circ$. (d–f) Optical image, SHG mapping, and atomic lattice model for GaSe bilayer with twist angle of $\phi = 60^\circ$. These results reveal that the Ga–Se bond direction is the same (opposite) in the parallel (antiparallel) triangular monolayers.

the angle between the angular bisector of each triangle. In our SHG mapping, we observed that $\phi = 0^\circ$ bilayer gives rise to enhanced SHG signal (Figure 4b), while the $\phi = 60^\circ$ bilayer gives nearly zero SHG signal (Figure 4e). This result reveals that the $\phi = 0^\circ$ bilayer belongs to the AA stacking (Figure 4c), while $\phi = 60^\circ$ bilayer belongs to the AB stacking (Figure 4f). Therefore, the Ga–Se bond directions in the parallel GaSe triangles are parallel to each other, instead of antiparallel.

The two facts that the monolayer GaSe triangle has a one-to-one correspondence to the lattice symmetry and the Ga–Se bond direction in the two parallel layers of GaSe bilayers is the same indicate that different triangular GaSe atomic layers may have the same dominant edge configurations. A direct experimental identification of the edge type of our CVD-grown sample can be obtained in the future by scanning tunneling microscope with a special conducting substrate that is compatible with GaSe CVD growth or by high-resolution transmission electron microscope³⁴ (but the electron beam irradiation may cause the reconstruction of the edge configuration³⁵).

In summary, we report the first observation of strong SHG in monolayer GaSe under nonresonant excitation and emission condition. The nonresonant SHG intensity of GaSe monolayer is the strongest among all the 2D atomic crystals measured up to day. Further polarization-dependent SHG intensity and SHG mapping reveal that the monolayer GaSe shows 3-fold lattice symmetry with an intrinsic correspondence to its geometric triangular shape in our growth condition; whereas the bilayer GaSe exhibits two dominant stacking orders: AA and AB stacking. Our observations also indicate that the dominant edge configuration in different GaSe triangles is the same. Our work demonstrates that the SHG spectroscopy can be potentially applied to study the in-plane grain boundary in monolayer GaSe or the stacking orders in few-layered GaSe. The strong nonlinear optical responses in mono- and few-layered GaSe also provide a platform to explore nonresonance properties of 2D materials.

■ ASSOCIATED CONTENT**■ Supporting Information**

Growth of GaSe monolayer and bilayers, SHG measurements, reflection spectrum measurements, and second-order nonlinear susceptibility calculation. The Supporting Information is available free of charge on the ACS Publications website at DOI: 10.1021/jacs.5b04305.

■ AUTHOR INFORMATION**Corresponding Authors**

*swwu@fudan.edu.cn

*hlpeng@pku.edu.cn

*khliu@pku.edu.cn

Author Contributions

[†]These authors contributed equally.

Notes

The authors declare no competing financial interest.

■ ACKNOWLEDGMENTS

This work was supported by the National Science Foundation of China (11474006, 91433102, 21173004), the National Basic Research Program of China (2014CB932500, 2014CB921600), and the National Program for Thousand Young Talents of China.

■ REFERENCES

- (1) Novoselov, K. S.; Geim, A. K.; Morozov, S. V.; Jiang, D.; Zhang, Y.; Dubonos, S. V.; Grigorieva, I. V.; Firsov, A. A. *Science* **2004**, *306*, 666.
- (2) Geim, A. K.; Novoselov, K. S. *Nat. Mater.* **2007**, *6*, 183.
- (3) Mak, K. F.; Lee, C.; Hone, J.; Shan, J.; Heinz, T. F. *Phys. Rev. Lett.* **2010**, *105*, 136805.
- (4) Splendiani, A.; Sun, L.; Zhang, Y. B.; Li, T. S.; Kim, J.; Chim, C. Y.; Galli, G.; Wang, F. *Nano Lett.* **2010**, *10*, 1271.
- (5) Wang, Q. H.; Kalantar-Zadeh, K.; Kis, A.; Coleman, J. N.; Strano, M. S. *Nat. Nanotechnol.* **2012**, *7*, 699.
- (6) Xia, F. N.; Wang, H.; Xiao, D.; Dubey, M.; Ramasubramanian, A. *Nat. Photonics* **2014**, *8*, 899.
- (7) Huang, X.; Zeng, Z.; Zhang, H. *Chem. Soc. Rev.* **2013**, *42*, 1934.
- (8) Huang, X.; Tan, C.; Yin, Z.; Zhang, H. *Adv. Mater.* **2014**, *26*, 2185.
- (9) Li, H.; Wu, J.; Yin, Z.; Zhang, H. *Acc. Chem. Res.* **2014**, *47*, 1067.
- (10) Tan, C.; Zhang, H. *Chem. Soc. Rev.* **2015**, *44*, 2713.
- (11) Yin, X.; Ye, Z.; Chenet, D. A.; Ye, Y.; O'Brien, K.; Hone, J. C.; Zhang, X. *Science* **2014**, *344*, 488.
- (12) Zhang, Y. J.; Oka, T.; Suzuki, R.; Ye, J. T.; Iwasa, Y. *Science* **2014**, *344*, 725.
- (13) Yu, H.; Wu, Y.; Liu, G. B.; Xu, X.; Yao, W. *Phys. Rev. Lett.* **2014**, *113*, 156603.
- (14) Late, D. J.; Liu, B.; Luo, J. J.; Yan, A. M.; Matte, H. S. S. R.; Grayson, M.; Rao, C. N. R.; Dravid, V. P. *Adv. Mater.* **2012**, *24*, 3549.
- (15) Hu, P. A.; Wen, Z. Z.; Wang, L. F.; Tan, P. H.; Xiao, K. *ACS Nano* **2012**, *6*, 5988.
- (16) Lei, S. D.; Ge, L. H.; Liu, Z.; Najmaei, S.; Shi, G.; You, G.; Lou, J.; Vajtai, R.; Ajayan, P. M. *Nano Lett.* **2013**, *13*, 2777.
- (17) Zhou, Y. B.; Nie, Y. F.; Liu, Y. J.; Yan, K.; Hong, J. H.; Jin, C. H.; Zhou, Y.; Yin, J. B.; Liu, Z. F.; Peng, H. L. *ACS Nano* **2014**, *8*, 1485.
- (18) Li, X. F.; Lin, M. W.; Puzos, A. A.; Idrobo, J. C.; Ma, C.; Chi, M. F.; Yoon, M.; Rouleau, C. M.; Kravchenko, I. I.; Geohegan, D. B.; Xiao, K. *Sci. Rep.* **2014**, *4*, 5497.
- (19) Rybkovskiy, D. V.; Arutyunyan, N. R.; Orekhov, A. S.; Gromchenko, I. A.; Vorobiev, I. V.; Osadchy, A. V.; Salaev, E. Y.; Baykara, T. K.; Allakhverdiev, K. R.; Obratsova, E. D. *Phys. Rev. B* **2011**, *84*, 085314.
- (20) Cao, T.; Li, Z.; Louie, S. G. *arXiv* **2014**, 1409, 4112.

(21) Segura, A.; Bouvier, J.; Andres, M. V.; Manjon, F. J.; Munoz, V. *Phys. Rev. B* **1997**, *56*, 4075.

(22) Allakhverdiev, K. R.; Yetis, M. O.; Ozbek, S.; Baykara, T. K.; Salaev, E. Y. *Laser Phys.* **2009**, *19*, 1092.

(23) Jie, W.; Chen, X.; Li, D.; Xie, L.; Hui, Y. Y.; Lau, S. P.; Cui, X.; Hao, J. *Angew. Chem., Int. Ed.* **2015**, *54*, 1185.

(24) Bube, R. H.; Lind, E. L. *Phys. Rev.* **1959**, *115*, 1159.

(25) Plucinski, L.; Johnson, R. L.; Kowalski, B. J.; Kopalko, K.; Orłowski, B. A.; Kovalyuk, Z. D.; Lashkarev, G. V. *Phys. Rev. B* **2003**, *68*, 125304.

(26) Li, Y. L.; Rao, Y.; Mak, K. F.; You, Y. M.; Wang, S. Y.; Dean, C. R.; Heinz, T. F. *Nano Lett.* **2013**, *13*, 3329.

(27) Kumar, N.; Najmaei, S.; Cui, Q. N.; Ceballos, F.; Ajayan, P. M.; Lou, J.; Zhao, H. *Phys. Rev. B* **2013**, *87*, 161403.

(28) Malard, L. M.; Alencar, T. V.; Barboza, A. P. M.; Mak, K. F.; de Paula, A. M. *Phys. Rev. B* **2013**, *87*, 201401.

(29) Hsu, W. T.; Zhao, Z. A.; Li, L. J.; Chen, C. H.; Chiu, M. H.; Chang, P. S.; Chou, Y. C.; Chang, W. H. *ACS Nano* **2014**, *8*, 2951.

(30) Jiang, T.; Liu, H.; Huang, D.; Zhang, S.; Li, Y.; Gong, X.; Shen, Y.-R.; Liu, W.-T.; Wu, S. *Nat. Nanotechnol.* **2014**, *9*, 825.

(31) Liu, K. H.; Zhang, L. M.; Cao, T.; Jin, C. H.; Qiu, D. A.; Zhou, Q.; Zettl, A.; Yang, P. D.; Louie, S. G.; Wang, F. *Nat. Commun.* **2014**, *5*, 4966.

(32) van der Zande, A. M.; Kunstrmann, J.; Chernikov, A.; Chenet, D. A.; You, Y. M.; Zhang, X. X.; Huang, P. Y.; Berkelbach, T. C.; Wang, L.; Zhang, F.; Hybertsen, M. S.; Muller, D. A.; Reichman, D. R.; Heinz, T. F.; Hone, J. C. *Nano Lett.* **2014**, *14*, 3869.

(33) Shen, Y. R. *The principles of nonlinear optics*; John Wiley & Sons, Inc.: Hoboken, NJ, 2003.

(34) Li, X.; Basile, L.; Yoon, M.; Ma, C.; Puzos, A. A.; Lee, J.; Idrobo, J. C.; Chi, M.; Rouleau, C. M.; Geohegan, D. B.; Xiao, K. *Angew. Chem., Int. Ed.* **2015**, *54*, 2712.

(35) Girit, C. O.; Meyer, J. C.; Erni, R.; Rossell, M. D.; Kisielowski, C.; Yang, L.; Park, C. H.; Crommie, M. F.; Cohen, M. L.; Louie, S. G.; Zettl, A. *Science* **2009**, *323*, 1705.